

Formation of Kaonic Atoms and Kaonic Nuclei in In-Flight (K^- , p) Reactions

Junko YAMAGATA¹, Hideko NAGAIHIRO², Yuko OKUMURA^{1,*} and Satoru HIRENZAKI¹

¹*Department of Physics, Nara Women's University, Nara 630-8506, Japan*

²*Research Center for Nuclear Physics(RCNP), Osaka University, Ibaraki, Osaka 567-0047, Japan*

(Received March 11, 2005)

We theoretically study kaonic atom and kaonic nucleus formation in in-flight (K^- , p) reactions for C, O, Si and Ca targets. Deeply bound kaonic atoms were previously predicted to exist as quasi-stable states, and it is expected that they can be observed using certain well-suited experimental methods. Kaonic nuclear states have also been predicted to exist with large decay widths. We evaluate the formation cross sections of kaonic atoms and kaonic nuclei using an effective number approach. We show that indications of kaonic bound states can be observed in the outgoing proton energy spectra.

§1. Introduction

Kaonic atoms and kaonic nuclei carry important information concerning the K^- -nucleon interaction in nuclear medium. This information is very important to determine the constraints on kaon condensation in high density matter. The properties of kaons in nuclei are strongly influenced by the change undergone by $\Lambda(1405)$ in nuclear medium, because $\Lambda(1405)$ is a resonance state just below the kaon-nucleon threshold. In fact, there are studies of kaonic atoms carried out by modifying the properties of $\Lambda(1405)$ in nuclear medium.^{1), 2), 3)} These works reproduce the properties of kaonic atoms very well, which come out to be as good as the phenomenological study of Batty.⁴⁾

Recently, there have been significant developments in the description of hadron properties in terms of the $SU(3)$ chiral Lagrangian. The unitarization of the chiral Lagrangian allows the interpretation of the $\Lambda(1405)$ resonance state as a baryon-meson coupled system.^{5), 6)} Subsequently, the properties of $\Lambda(1405)$ in nuclear medium using the $SU(3)$ chiral unitary model were also investigated by Waas et al.,⁷⁾ Lutz,⁸⁾ Ramos and Oset,⁹⁾ and Cieplý et al.¹⁰⁾ All of these works considered the Pauli effect on the intermediate nucleons. In addition, in Ref. 8), the self-energy of the kaon in the intermediate states is considered, and in Ref. 9), the self-energies of the pions and baryons are also taken into account. These approaches lead to a kaon self-energy in nuclear medium that can be tested with kaonic atoms and kaonic nuclei. There are also \bar{K} potential studies based on meson-exchange Jülich $\bar{K}N$ interaction.^{11), 12)}

In a previous work,¹³⁾ we adopted the scattering amplitude in nuclear medium calculated by Ramos and Oset⁹⁾ for studies of kaonic atoms, and demonstrated

*) Present address: Ritto High School, Ritto, Shiga, Japan

the ability to reproduce the existing kaonic atom data as accurately as the optical potential studied by Batty.⁴⁾ We then calculated the deeply bound kaonic atoms for ^{16}O and ^{40}Ca , which have narrow widths and are believed to be observable with well-suited experimental methods.^{14), 15)} We also obtained very deep kaonic nuclear states, which have large decay widths, of the order of several tens of MeV. The (K^-, γ) reaction was studied for the formation of the deeply bound kaonic atomic states,¹³⁾ which could not be observed with kaonic X-ray spectroscopy, using the formulation developed in Ref. 16) for the formation of deeply bound pionic atoms with the (π^-, γ) reaction.

Another very important development in recent years is that in the study of kaonic nuclear states, which are kaon-nucleus bound systems determined mainly by the strong interaction. Experimental studies of the kaonic nuclear states using in-flight (K, N) reactions were proposed and performed by Kishimoto and his collaborators.^{17), 18)} Experiments employing stopped (K, N) reactions were carried out by Iwasaki, T. Suzuki and their collaborators and reported in Refs. 19) and 20). In these experiments, they found some indications of the existence of kaonic nuclear states. There are also theoretical studies of the structure and formation of kaonic nuclear states related to these experimental activities.²¹⁾ It should be noted that these theoretical studies predict the possible existence of ultra-high density states in kaonic nuclear systems.^{21), 22)}

In this paper, we study in-flight (K^-, p) reactions systematically with regard to their role in populating deeply bound kaonic states and the observation of their properties in experiments. We have found the usefulness of direct reactions in the formation of deeply bound pionic atoms using the $(d, ^3\text{He})$ reactions.^{23), 24), 25), 26)} However, in the present case, K^+ must be produced in addition in this $(d, ^3\text{He})$ reaction, and there would be a large momentum mismatch. For this reason, the (K^-, γ) reaction was considered first in Ref. 13). Here we theoretically study another reaction, (K^-, p) , and present systematic results that elucidate the experimental feasibility of the reaction. The (K^-, p) reaction was proposed in Refs. 15) and 17). However, realistic spectra have not yet been calculated. We calculate the spectra theoretically using the approach of Ref. 24) for the deeply bound pionic atom formation reaction. We believe that this theoretical evaluation will be interesting and important for studies of kaon properties in nuclear medium.

In §2, we describe the theoretical model of the structure of kaon-nucleus bound systems and present the numerical results. The theoretical formalism and numerical results for the (K^-, p) reactions are discussed in §3. We give summary in §4.

§2. Structure of kaonic atoms and kaonic nuclei

2.1. Formalism

We study the properties of kaonic bound systems by solving the Klein-Gordon equation

$$[-\nabla^2 + \mu^2 + 2\mu V_{\text{opt}}(r)]\phi(\mathbf{r}) = [E - V_{\text{coul}}(r)]^2\phi(\mathbf{r}) . \quad (2\cdot 1)$$

Here, μ is the kaon-nucleus reduced mass and $V_{\text{coul}}(r)$ is the Coulomb potential with a finite nuclear size:

$$V_{\text{coul}}(r) = -e^2 \int \frac{\rho_p(r')}{|\mathbf{r}-\mathbf{r}'|} d^3r', \quad (2.2)$$

where $\rho_p(r)$ is the proton density distribution. We employ the empirical Woods-Saxon form for the density and keep the shapes of the neutron and proton density distributions fixed as

$$\rho(r) = \rho_n(r) + \rho_p(r) = \frac{\rho_0}{1 + \exp[(r - R)/a]}, \quad (2.3)$$

where we use $R = 1.18A^{1/3} - 0.48$ [fm] and $a = 0.5$ [fm] with A , the nuclear mass number. It is noticed that the point nucleon density distributions are deduced from ρ in Eq. (2.3) by using the same prescription described in Sect. 4 in Ref. 29) and are used to evaluate the kaon-nucleus optical potential.

The kaon-nucleus optical potential V_{opt} is given by

$$2\mu V_{\text{opt}}(r) = -4\pi\eta a_{\text{eff}}(\rho)\rho(r), \quad (2.4)$$

where $a_{\text{eff}}(\rho)$ is a density dependent effective scattering length and $\eta = 1 + m_K/M_N$. In this paper, we use two kinds of effective scattering lengths, that obtained with the chiral unitary approach⁹⁾ and that obtained with a phenomenological fit.²⁷⁾ Here, we do not introduce any energy dependence for the effective scattering lengths, and we use the scattering lengths at the KN threshold energy. The effective scattering length a_{eff} of the chiral unitary approach is described in Ref. 13) in detail. It is defined by the kaon self-energy in nuclear matter, with the local density approximation. The form of a_{eff} obtained in a phenomenological fit is one of the results reported in Ref. 27), and it is parameterized as

$$a_{\text{eff}}(\rho) = (-0.15 + 0.62i) + (1.66 - 0.04i)(\rho/\rho_0)^{0.24}[\text{fm}]. \quad (2.5)$$

The reason we consider these two potentials is that they provide equivalently good descriptions of the observed kaonic atom data, even though they have very different potential depths, as we will see in next subsection. Thus, it should be extremely interesting to compare the results obtained with these potentials in the (K^- , p) reaction spectra, including the kaonic nuclear region.

We solve the Klein-Gordon equation numerically, following the method of Oset and Salcedo.²⁸⁾ The application of this method to pionic atom studies are reported in detail in Ref. 29).

2.2. Numerical results

We show the kaon nucleus potential for the ^{39}K case in Fig. 1 as an example. Because the real part of $a_{\text{eff}}(\rho)$ changes sign at a certain nuclear density in both the chiral unitary and phenomenological models, the kaon nucleus optical potential is attractive, while keeping the repulsive sign for the kaon-nucleon scattering length in free space.

The real part of the scattering length for the phenomenological fit depends on the density much more strongly than the results of the chiral unitary model and

yields $\text{Re } a_{\text{eff}}(\rho_0) = 1.51[\text{fm}]$. Hence, as we can see in Fig. 1, the depths of the real optical potentials of these models differ significantly. On the other hand, the density dependence of the imaginary part of the phenomenological scattering length is rather flat, and its strength is similar to that of the chiral unitary model.

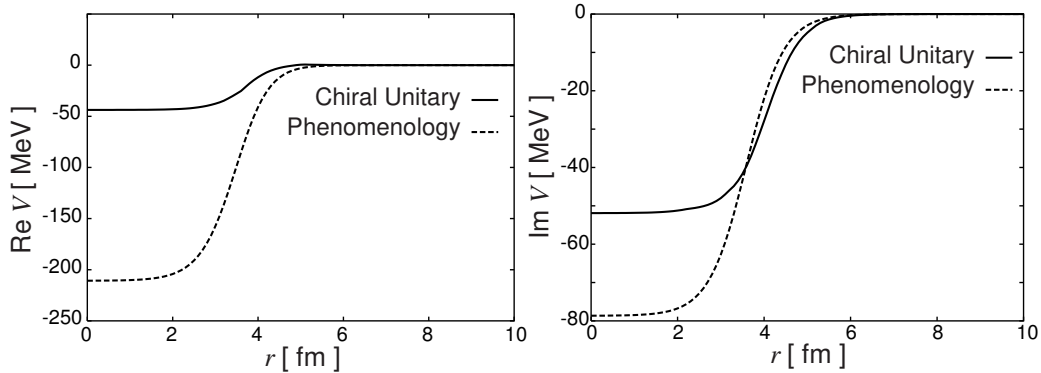


Fig. 1. The kaon-nucleus optical potential for ^{39}K as a function of the radial coordinate r . The left and right panels show the real and imaginary part, respectively. The solid line indicates the potential strength of the chiral unitary approach and the dashed line of the phenomenological fit.

The calculated energy levels for the atomic states and nuclear states in ^{39}K are shown in Fig. 2, where the results of the chiral model and the phenomenological model, Eq. (2.5), are compared. We see that the results obtained with the two potentials are very similar for the atomic states. We find that the deep atomic states, such as atomic $1s$ in ^{39}K (still unobserved), appear with narrower widths than the separation between levels and are predicted to be quasi-stable states. Similar results are reported in previous works.^{13),14)} Because several model potentials predict the existence of quasi-stable deep atomic states, it would be interesting to observe the states experimentally. On the other hand, the predicted binding energies and widths are very stable and almost identical for all of the potential models considered here. Hence, it is very difficult to distinguish the theoretical potentials from only the observation of atomic levels.

In the lower panels of Fig. 2, we also show the energy levels of the deep nuclear kaonic states of ^{39}K using the chiral unitary model potential and the phenomenological model potential. The deep nuclear states are represented by the solid bars with numbers, which indicate their widths in units of MeV. These nuclear states have extremely large widths in all cases and would not be observed as peak structures in experiments if they indeed do have such large widths. We should, however, mention here that the level structures of these potential models differ significantly. In the chiral unitary potential, only two nuclear states are predicted, while eight states are predicted with the phenomenological model. This difference presents the opportunity to distinguish the theoretical potentials in observations of kaonic nuclear states.

Calculated density distributions of nuclear $1s$ and $2s$ and atomic $1s$ kaonic states in ^{39}K are shown in Fig. 3 for the case of the phenomenological optical potential.

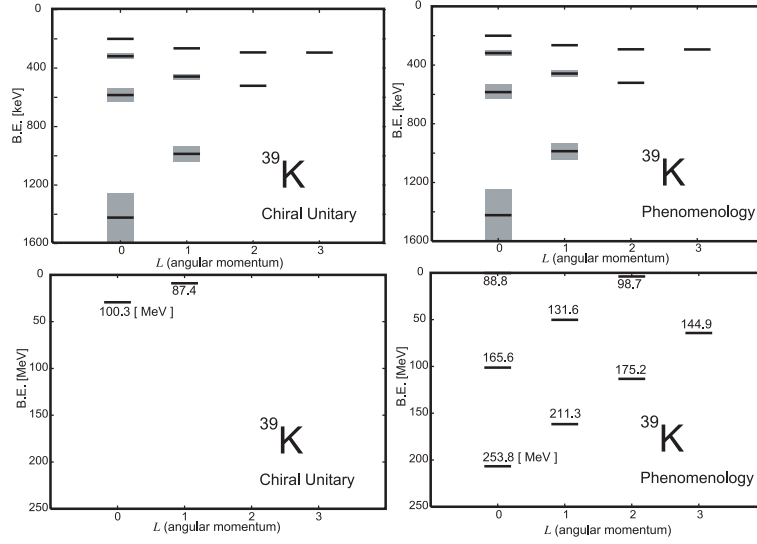


Fig. 2. (Upper panel) Energy levels of kaonic atoms of ^{39}K obtained with the optical potentials of the chiral unitary model (left) and the phenomenological fit (right). The hatched areas indicate the level widths. (Lower panel) Energy levels of kaonic nuclear states of ^{39}K obtained with the optical potentials of the chiral unitary model (left) and the phenomenological fit (right). The level width is indicated by the number appearing at each level, in units of MeV.

It is seen that the wavefunctions of the deep nuclear kaonic states remain almost entirely inside the nuclear radius, which is about 3.5 fm for ^{39}K . Hence, the widths become extremely large, of the order of 100 MeV. The wavefunctions of the atomic states are pushed outward by the imaginary part of the strong interaction. It should be noted that the atomic $1s$ state corresponds to the 4-th s state in the solutions of the Klein-Gordon (KG) equation, Eq. (2-1). We divided the series of KG solutions into two categories, 'atomic states' and 'nuclear states', since the properties of these states are very different, and there are no ambiguities in this classification, as can be seen in Figs. 2 and 3.

We have also calculated the kaon-nucleus binding energies and widths for both atomic and nuclear states in other nuclei. The obtained results are compiled in Tables I and II for the phenomenological optical potential and for the chiral unitary potential cases, respectively. We selected ^{11}B , ^{15}N , ^{27}Al and ^{39}K nuclei, which appear in the final states of the formation reactions for ^{12}C , ^{16}O , ^{28}Si and ^{40}Ca targets, as described in the next section. In all cases, we found kaonic atom states and kaonic nuclear states. The results for the atomic states are similar for the two potentials and are known to reproduce existing data reasonably well. On the other hand, certain differences are found in the energy spectra of kaonic nuclear states, as expected, and they should be investigated experimentally.

We should mention here that the kaonic nuclear $2p$ state in ^{27}Al described in Table II provides a negative value for the binding energy. This state, however, is interpreted as a bound state, since the sign of the corresponding eigenenergy in the non-relativistic Schrödinger equation is opposite to that of the Klein-Gordon

Table I. Calculated binding energies and widths of kaon- ^{11}B , ^{-15}N , ^{-27}Al and ^{-39}K systems with the phenomenological optical potential in units of MeV for kaonic nuclear states and in units of keV for kaonic atom states.

Nuclear State (MeV)	^{11}B		^{15}N		^{27}Al		^{39}K	
	B.E.	Γ	B.E.	Γ	B.E.	Γ	B.E.	Γ
1s	132.5	183.0	155.7	205.5	190.8	239.5	206.7	253.8
2s	-	-	19.0	96.2	69.8	142.3	101.3	165.6
3s	-	-	-	-	-	-	2.1×10^{-1}	88.8
2p	58.4	127.0	86.9	151.1	136.3	191.2	161.7	211.3
3p	-	-	-	-	16.5	103.3	50.2	131.6
3d	-	-	22.9	108.3	80.4	152.2	113.3	175.2
4d	-	-	-	-	-	-	3.9	98.7
4f	-	-	-	-	26.2	119.5	64.3	144.9
Atomic State (keV)								
1s	192.4	40.6	338.1	68.3	844.9	243.1	1408.0	355.4
2s	60.5	7.3	111.8	13.3	319.0	58.3	580.6	97.6
3s	29.2	2.5	55.1	4.6	166.8	22.3	316.9	39.9
4s	17.1	1.1	21.7	1.1	102.3	10.8	199.4	20.0
2p	78.5	6.2×10^{-1}	154.6	4.0	507.5	37.4	988.7	132.7
3p	34.9	2.2×10^{-1}	68.8	1.4	229.4	12.7	458.4	45.8
4p	19.6	9.6×10^{-2}	38.7	6.1×10^{-1}	130.5	5.7	265.1	20.8
3d	34.9	2.3×10^{-4}	69.3	2.9×10^{-3}	243.0	4.2×10^{-1}	520.9	5.0
4d	19.6	1.4×10^{-4}	39.0	1.7×10^{-3}	136.6	2.5×10^{-1}	292.6	2.9
4f	19.6	1.0×10^{-8}	38.9	4.8×10^{-7}	136.5	3.2×10^{-4}	293.7	1.7×10^{-2}

Table II. Calculated binding energies and widths of kaon- ^{11}B , ^{-15}N , ^{-27}Al and ^{-39}K systems with the optical potential of the chiral unitary model, in units of MeV for kaonic nuclear states and in units of keV for kaonic atom states.

Nuclear State (MeV)	^{11}B		^{15}N		^{27}Al		^{39}K	
	B.E.	Γ	B.E.	Γ	B.E.	Γ	B.E.	Γ
1s	4.6	81.6	11.0	87.9	22.5	96.6	29.3	100.3
2p	-	-	-	-	-1.1	79.5	9.0	87.4
Atomic State (keV)								
1s	197.5	35.0	340.5	67.8	852.1	199.1	1422.7	337.3
2s	61.3	6.2	112.3	13.2	320.4	47.6	584.3	92.5
3s	29.5	2.1	55.3	1.6	167.2	18.2	318.3	37.8
4s	17.3	9.3×10^{-1}	21.7	1.1	102.5	8.8	200.1	19.0
2p	78.4	6.3×10^{-1}	154.4	3.1	507.3	34.8	986.8	109.3
3p	34.8	2.2×10^{-1}	68.7	1.1	229.3	11.8	457.7	37.7
4p	19.6	9.7×10^{-2}	38.7	4.8×10^{-1}	130.5	5.3	264.8	17.1
3d	34.9	1.6×10^{-4}	69.3	2.6×10^{-3}	243.0	3.4×10^{-1}	520.8	4.5
4d	19.6	9.5×10^{-5}	39.0	1.6×10^{-3}	136.6	2.0×10^{-1}	292.6	2.6
4f	19.6	1.0×10^{-8}	38.9	3.7×10^{-7}	136.5	2.8×10^{-4}	293.7	1.5×10^{-2}

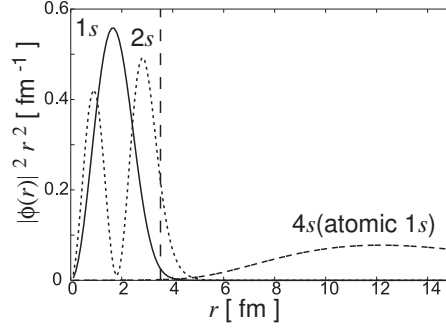


Fig. 3. The kaonic bound state density distributions $|\phi(r)|^2$ in coordinate space for ^{39}K obtained with the phenomenological optical potential. The solid and dotted curves indicate the distributions of the $1s$ and $2s$ states. The dashed curve represents the density of the $4s$ state and is regarded as a kaonic atom $1s$ state. The half-density radius of ^{39}K is also shown.

solution, due to the large widths of the nuclear states, as shown below. The binding energies B_{KG} and widths Γ_{KG} of the Klein-Gordon equation, which are tabulated in Tables I and II, are defined as $E = (\mu - B_{\text{KG}}) - \frac{i}{2}\Gamma_{\text{KG}}$ by the eigenenergy E in Eq. (2.1). The non-relativistic binding energy B_{S} and width Γ_{S} of the Schrödinger equation are related to B_{KG} and Γ_{KG} as

$$B_{\text{S}} = B_{\text{KG}} - \frac{B_{\text{KG}}^2}{2\mu} + \frac{\Gamma_{\text{KG}}^2}{8\mu}, \quad (2.6)$$

$$\Gamma_{\text{S}} = \Gamma_{\text{KG}} - \frac{B_{\text{KG}}}{\mu} \Gamma_{\text{KG}}. \quad (2.7)$$

Thus, in the case of the kaonic $2p$ nuclear state in ^{27}Al described in Table II, the non-relativistic binding energies and widths are $B_{\text{S}} \sim 0.5\text{MeV}$ and $\Gamma_{\text{S}} \sim \Gamma_{\text{KG}}$, which indicate that the state is bound. It should be noted that the asymptotic behavior of the wavefunction is determined by B_{S} .

§3. Kaonic atoms and kaonic nuclei formation in (K^- , p) reactions

3.1. Formalism

We adopt the theoretical model presented in Ref. 24) to calculate the formation cross sections of the kaonic atoms and kaonic nuclei in the (K^- , p) reaction. In this model, the emitted proton energy spectra can be written as

$$\frac{d^2\sigma}{dE_p d\Omega_p} = \left(\frac{d\sigma}{d\Omega} \right)_{K^-p \rightarrow pK^-}^{\text{lab}} \sum_f \frac{\Gamma_K}{2\pi} \frac{1}{\Delta E^2 + \Gamma_K^2/4} N_{\text{eff}}, \quad (3.1)$$

where the sum is over all (kaon-particle) \otimes (proton-hole) configurations in the final kaonic bound states. The differential cross section for the elementary process of the reaction $K^- + p \rightarrow p + K^-$ in the laboratory frame, $(d\sigma/d\Omega)_{K^-p \rightarrow pK^-}^{\text{lab}}$ is evaluated using the K^-p total elastic cross section data in Ref. 30) by assuming a flat angular

distribution in the center-of-mass frame at each energy. The resonance peak energy is determined by ΔE appearing in Eq. (3.1), which is defined as

$$\Delta E = T_p - (T_K - S_p(j_p^{-1}) + B_K), \quad (3.2)$$

where T_K is the incident kaon kinetic energy, T_p the emitted proton kinetic energy, and B_K the kaon binding energy in the final state. The proton separation energy S_p from each single particle level listed in Table III is obtained from the data in Refs. 31), 32), 33), 34), 35), 36). We use the data in Ref. 37) for the separation energies of the proton-hole levels corresponding to the ground states of the daughter nuclei. The widths of the hole states Γ_p are also listed in Table III. These were obtained from the same data sets by assuming the widths of the ground states of the daughter nuclei to be zero because of their stabilities.

Table III. One proton separation energies S_p and widths Γ_p of the hole states of ^{12}C , ^{16}O , ^{28}Si and ^{40}Ca deduced from the data given in Ref. 31) for ^{12}C , those given in Refs. 32) and 33) for ^{16}O , those given in Refs. 34) and 35) for ^{28}Si , and those given in Ref. 36) for ^{40}Ca . The separation energies corresponding to the ground states of the daughter nuclei are taken from Ref. 37). The widths Γ_p indicate FWHM of the Lorentz distribution for ^{16}O and of Gaussian distributions for other nuclei. The widths of the ground states of the daughter nuclei are fixed to zero, because of their stabilities. For the $1p$ states in ^{28}Si and ^{40}Ca , two levels, $1p_{1/2}$ and $1p_{3/2}$, have not been observed separately, and therefore S_p and Γ_p are set to the same values for both levels.

single particle states [MeV]	^{12}C		^{16}O		^{28}Si		^{40}Ca	
	S_p	Γ_p	S_p	Γ_p	S_p	Γ_p	S_p	Γ_p
$1d_{3/2}$							8.3	0
$2s_{1/2}$							11.5	7.7
$1d_{5/2}$					11.6	0	16.3	3.7
$1p_{1/2}$			12.1	0	27.5	17.0	33.2	21.6
$1p_{3/2}$	16.0	0	18.4	3.1×10^{-6}	27.5	17.0	33.2	21.6
$1s_{1/2}$	33.9	12.1	41.1	19.0	46.5	21.0	56.3	30.6

The effective number N_{eff} is defined as

$$N_{\text{eff}} = \sum_{JMm_s} \left| \int d^3r \chi_f^*(\mathbf{r}) \xi_{1/2, m_s}^* [\phi_{l_K}^*(\mathbf{r}) \otimes \psi_{j_p}(\mathbf{r})]_{JM} \chi_i(\mathbf{r}) \right|^2. \quad (3.3)$$

The proton and the kaon wavefunctions are denoted by ψ_{j_p} and ϕ_{l_K} . We adopt the harmonic oscillator wavefunction for ψ_{j_p} . The spin wave function is denoted by $\xi_{1/2, m_s}$, and we take the spin average with respect to m_s , so as to take into account the possible spin directions of the protons in the target nucleus. The functions χ_i and χ_f are the initial and final distorted waves of the projectile and ejectile, respectively. We use the eikonal approximation and replace χ_f and χ_i by employing the relation

$$\chi_f^*(\mathbf{r}) \chi_i(\mathbf{r}) = \exp(i\mathbf{q} \cdot \mathbf{r}) D(z, \mathbf{b}), \quad (3.4)$$

where \mathbf{q} is the momentum transfer between the projectile and ejectile, and the distortion factor $D(z, \mathbf{b})$ is defined as

$$D(z, \mathbf{b}) = \exp \left[-\frac{1}{2} \sigma_{KN} \int_{-\infty}^z dz' \rho_A(z', \mathbf{b}) - \frac{1}{2} \sigma_{pN} \int_z^{\infty} dz' \rho_{A-1}(z', \mathbf{b}) \right]. \quad (3.5)$$

Here, the kaon-nucleon and proton-nucleon total cross sections are denoted by σ_{KN} and σ_{pN} . The functions $\rho_A(z, \mathbf{b})$ and $\rho_{A-1}(z, \mathbf{b})$ are the density distributions of the target and daughter nuclei in the beam direction coordinate z with impact parameter \mathbf{b} , respectively.

We calculated the kaonic bound state wavefunctions using the optical potentials obtained with the chiral unitary model¹³⁾ and the phenomenological fit,²⁷⁾ as described in §2. In the chiral unitary model, the depth of the attractive potential is only approximately 50 MeV at the center of the nucleus, which is much weaker than the phenomenological potential used in Ref. 27). For the case of the phenomenological potential, there exist kaonic nuclear bound states with very large binding energies, for example, 100 – 200 MeV. For these bound states, the $\bar{K}N$ system cannot decay into $\pi\Sigma$, because of the threshold, and hence, the widths of these states are expected to be narrower. On the other hand, for chiral unitary potential cases, we do not have narrow nuclear states, like those in Refs. 17) and 21), because the decay phase space for the $\bar{K}N$ system to the $\pi\Sigma$ channel is sufficiently large, owing to the smaller binding energies. In order to include 'narrowing effects' for the widths due to the phase space suppression, we introduce a phase space factor f^{MFG} , defined in Ref. 38) by Mareš, Friedman, and Gal as,

$$f^{\text{MFG}}(E) = 0.8f_1^{\text{MFG}}(E) + 0.2f_2^{\text{MFG}}(E), \quad (3.6)$$

where f_1^{MFG} and f_2^{MFG} are the phase space factors for $\bar{K}N \rightarrow \pi\Sigma$ decay and $\bar{K}NN \rightarrow \Sigma N$, respectively. These factors are defined as

$$f_1^{\text{MFG}}(E) = \frac{M_{01}^3}{M_1^3} \sqrt{\frac{[M_1^2 - (m_\pi + m_\Sigma)^2][M_1^2 - (m_\Sigma - m_\pi)^2]}{[M_{01}^2 - (m_\pi + m_\Sigma)^2][M_{01}^2 - (m_\Sigma - m_\pi)^2}}} \theta(M_1 - m_\pi - m_\Sigma), \quad (3.7)$$

and

$$f_2^{\text{MFG}}(E) = \frac{M_{02}^3}{M_2^3} \sqrt{\frac{[M_2^2 - (m_N + m_\Sigma)^2][M_2^2 - (m_\Sigma - m_N)^2]}{[M_{02}^2 - (m_N + m_\Sigma)^2][M_{02}^2 - (m_\Sigma - m_N)^2}}} \theta(M_2 - m_\Sigma - m_N). \quad (3.8)$$

Here, the branching ratios of mesic decay and non-mesic decay are assumed to be 80% and 20%. The masses are defined as $M_{01} = m_{\bar{K}} + m_N$, $M_1 = M_{01} + E$, $M_{02} = m_{\bar{K}} + 2m_N$, $M_2 = M_{02} + E$, and E is the kaon energy defined as $E = T_K - T_p - S_p$, using the same kinematical variables as in Eq. (3.2). We multiply the energy independent kaonic widths Γ_K by the phase space factor f^{MFG} in order to introduce the energy dependence due to the phase space suppression as

$$\Gamma_K \rightarrow \Gamma_K(E) = \Gamma_K \times f^{\text{MFG}}(E). \quad (3.9)$$

3.2. Numerical results

We present the numerical results for the kaon bound state formation spectra in this subsection. First, we consider the momentum transfer of the (K^-, p) reactions as a function of the incident kaon energy, which is an important guide to determine suitable incident energies in order to obtain a large production rate of the bound states. Because we consider both atomic and nuclear kaon states, we assume four different binding energies to calculate the momentum transfer. We consider the forward reactions and the momentum transfer in the laboratory frame, as shown in Fig. 4. As can be seen in the figure, the condition of zero recoil can be satisfied only for atomic states with $T_K = 10 - 20$ MeV. For deeply bound nuclear states, the reaction always requires a certain momentum transfer. However, the incident energy dependence of the momentum transfer is not strong for kaonic nuclear states, as shown in Fig. 4.

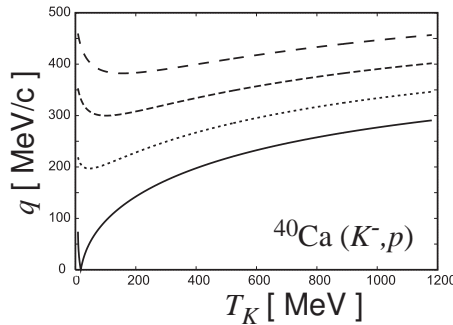


Fig. 4. Momentum transfers in the (K^-, p) reactions with ^{40}Ca for targets the formation of kaon- ^{39}K bound systems. The proton separation energy S_p is fixed at 8.3 MeV, and the kaon binding energies are assumed to be 0 MeV (solid curve), 50 MeV (dotted curve), 100 MeV (dashed curve), and 150 MeV (long-dashed curve).

We consider formation of kaonic atoms and kaonic nuclei separately, because their properties, and hence, the optimal kinematical conditions for their formation are expected to be different. We first consider the formation of atomic states. Because the binding energies of atomic states are sufficiently small, we can safely ignore the phase space effect for the decay widths considered in Eqs. (3.6) – (3.9). For atomic states, the obtained wavefunctions and energy spectra are almost identical for the chiral unitary and phenomenological potentials. For this reason, we show the results only for chiral unitary potential.

We first study the energy dependence of the atomic $1s$ state formation rate in order to determine the optimal incident energy for the deepest atomic $1s$ state observation in the (K^-, p) reactions. For this purpose, we show in Fig. 5 the energy dependence of the ratio of the calculated effective numbers of the kaonic atom $1s$ and $2p$ states coupled to the $[d_{3/2}^{-1}]$ proton-hole state in ^{39}K . We find that the contribution of the $1s$ state is significantly larger than that of the $2p$ state at $T_K = 20$ MeV, and we therefore hypothesize that the $1s$ state can be observed clearly without a large background due to the $2p$ kaonic state at this energy, where the momentum

transfer is reasonably small for atomic state formation. Next, we consider the energy dependence of the peak height of the $1s$ kaonic atom state coupled to the $[d_{3/2}^{-1}]$ proton-hole state in ^{39}K to determine the suitable incident energy to have a large cross section. As we can see in Fig. 6, the cross section is maximal somewhere in the range $T_K = 30 - 40$ MeV, and we find that the cross section has a local maximum value near $T_K = 400$ MeV. From these observations, we take $T_K = 20$ and 400 MeV as the incident kaon energies to calculate the energy spectrum of the emitted proton. We also consider $T_K = 100$ MeV as an energy between 20 and 400 MeV. We mention here that the eikonal approximation is known to be valid only for high energies. Thus, the results for low energies, i.e. $T_K \leq 100$ MeV, should be regarded as rough estimations.

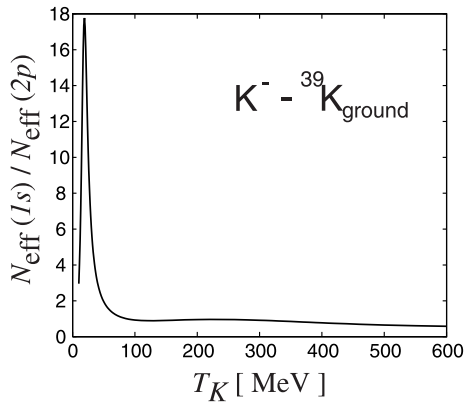


Fig. 5. Ratio of the effective numbers of $1s$ and $2p$ kaonic atom states formed with the $[d_{3/2}^{-1}]$ proton-hole state in ^{39}K plotted as a function of the incident kaon energy T_K .

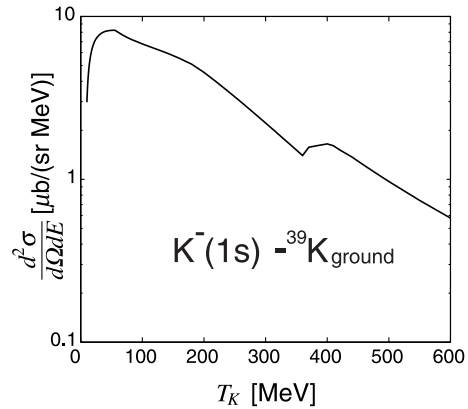


Fig. 6. Double differential cross section at the resonance peak energy of the kaonic atom $1s$ state formation with the $[d_{3/2}^{-1}]$ proton-hole state in ^{39}K at $\theta_p^{\text{Lab}} = 0$ [degrees] plotted as a function of the incident kaon kinetic energy.

In Fig. 7 we show the calculated spectra for a ^{40}Ca target, including contributions from the kaonic atom states up to $4f$ for $[1d_{3/2}^{-1}]$, $[1d_{5/2}^{-1}]$ and $[2s_{1/2}^{-1}]$ proton states in ^{39}K at $T_K = 20$ MeV. The spectra without the widths of the proton-hole states Γ_p are represented by the dashed curve. We find that the contributions coupled to different proton-hole states are localized in different energy regions and are well separated from each other. This feature of the spectra is different from that of the pionic atom formation in the $(d, ^3\text{He})$ reaction,²⁴⁾ where the contributions from different neutron-hole states overlap. We find the same features of the spectra for other incident energies.³⁹⁾ The realistic spectra including Γ_p are plotted by the solid lines in the same figure. As can be seen in the figure, Γ_p is too large to identify each kaonic bound state, except for the $[d_{3/2}^{-1}]$ hole state, corresponding to the ground state of the final daughter nucleus ^{39}K .

We show in Fig. 8 the detailed structure of the kaonic atom formation cross section coupled to the ground state of the daughter nucleus ^{39}K . Contributions from deeper proton-hole states provide the smooth background of the spectra in this

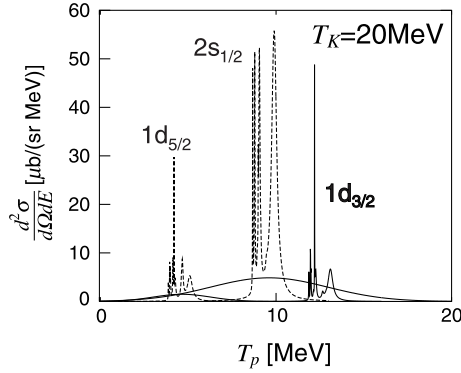


Fig. 7. Kaonic atom formation cross sections for each proton-hole state in the (K^-, p) reactions plotted as functions of the emitted proton energy at the incident kaon energy $T_K = 20$ MeV and $\theta_p^{\text{Lab}} = 0$ [degrees]. The solid and dashed curves are results with and without the widths of the proton-hole states, respectively.

energy region because of their large widths. We find that the contributions from deeply bound $1s$ and $2p$ kaonic atom states are well separated. At $T_K = 20$ MeV, the peak due to the $1s$ state is significantly larger than that due to the $2p$ state, as expected from the result in Fig. 5. The peak height of the atomic $1s$ contribution is approximately $7 [\mu\text{b}/(\text{sr MeV})]$ at $T_K = 20$ and 100 MeV. At $T_K = 100$ MeV, the $2p$ peak is enhanced and is approximately $24 [\mu\text{b}/(\text{sr MeV})]$. The overall shapes of the cross sections at 100 MeV and 400 MeV are similar, while the absolute strength at 400 MeV is approximately $1/3 - 1/4$ of that at 100 MeV. We should mention here that the energy resolution of experiments must be good enough so as to observe the separate peak structure in the spectrum for the atomic states formation.

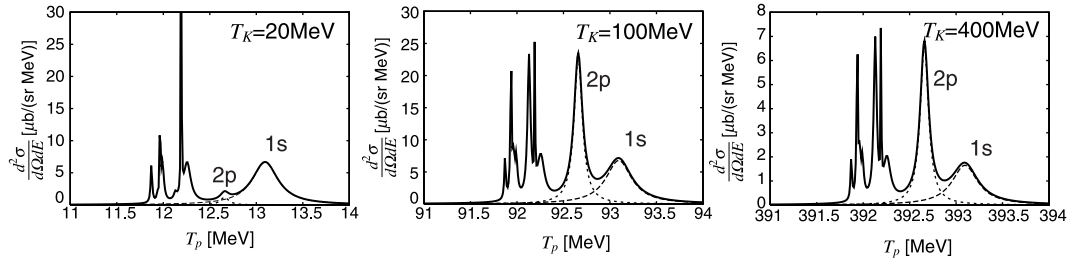


Fig. 8. Kaonic atom formation cross sections in $^{40}\text{Ca}(K^-, p)$ reactions coupled to the $[d_{3/2}^{-1}]$ proton-hole state in ^{39}K plotted as functions of the emitted proton energy at $\theta_p^{\text{Lab}} = 0$ [degrees] at the incident kaon energies $T_K = 20$ MeV, 100 MeV and 400 MeV, respectively.

We next consider the formation spectra of the kaonic nuclear states in the (K^-, p) reactions. We choose the incident kaon energy to be $T_K = 600$ MeV, for which there exist experimental data.¹⁸⁾ We show in Fig. 9 the formation spectra of kaonic nuclei together with those of kaonic atoms as functions of the emitted proton kinetic energies. Here, the widths of the kaonic states are fixed to the values listed in Tables I and II. The effects of the proton-hole widths Γ_p are included. We found that the spectra do not exhibit any peak-like structure due to the nuclear state formation but

have only a smooth slope in both the chiral unitary and phenomenological optical potential cases. The contributions from the atomic state formation appear as two very narrow peaks around, the threshold energies for both potentials. Each large peak contains several smaller peaks, due to the formation of several atomic states, as in the spectrum shown in Fig. 8.

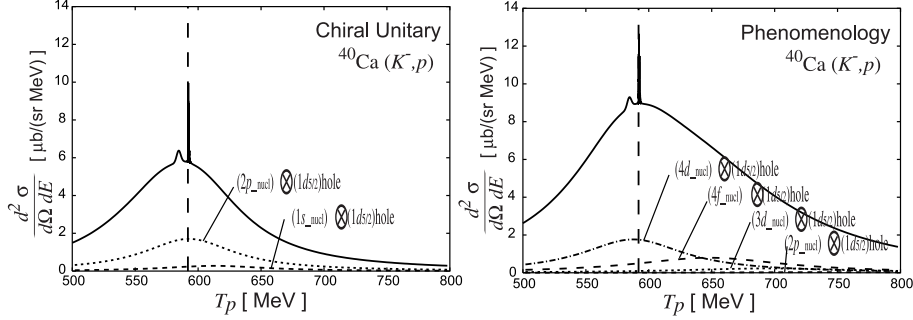


Fig. 9. Kaonic nucleus formation cross sections in $^{40}\text{Ca}(K^-, p)$ reactions plotted as functions of the emitted proton energies at $\theta_p^{\text{Lab}} = 0$ [degrees] and $T_K = 600$ MeV for (left) the chiral unitary model and (right) the phenomenological K -nucleus optical potential. The vertical dashed lines indicate the threshold energies, and the sharp peaks around the threshold are due to the atomic state formations.

In order to include the phase space effects on the decay widths for the final kaon system, we multiply the widths of kaonic states Γ_K by the phase space factor defined in Eqs. (3.6)–(3.9) and calculate the (K^-, p) spectra. We present the results in Fig. 10 for both potentials. We find that the spectrum for the chiral unitary potential is not affected significantly by the phase space effect. However, the (K^-, p) spectrum shape for the phenomenological potential is distorted by including the phase space factor and is expected to possess a bumpy structure, as reported in Ref. 18).

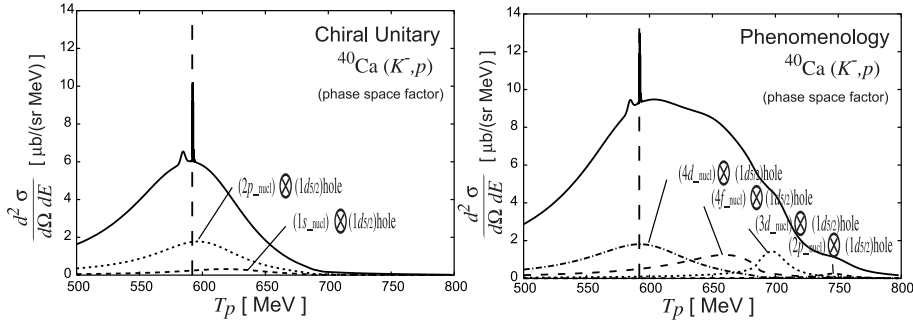


Fig. 10. Kaonic nucleus formation cross sections in $^{40}\text{Ca}(K^-, p)$ reactions plotted as functions of the emitted proton energies at $\theta_p^{\text{Lab}} = 0$ [degrees] and $T_K = 600$ MeV for (left) the chiral unitary model and (right) the phenomenological K -nucleus optical potential. The vertical dashed lines indicate the threshold energies, and the sharp peaks around the threshold are due to the atomic state formations. The energy dependent decay widths for kaonic states are used. (See the main text in details.)

We performed systematic calculations for other target nuclei, ^{12}C , ^{16}O and ^{28}Si

at $T_K = 600$ MeV and present the results in Fig. 11. In Ref. 18), experimental data for a ^{16}O target are reported and data for ^{12}C and ^{28}Si targets could be obtained in the future.⁴⁰⁾ As shown in Fig. 11, we have found that some bumpy structures in the (K^-, p) spectra may appear, due to the formation of the kaon nucleus states, especially in the case of the ^{12}C target, if the kaon-nucleus optical potential is as deep as 200 MeV, as reported in Ref. 27). On the other hand, if the depth of the optical potential is as shallow as 50 MeV, as predicted by the chiral unitary model, the spectrum may not possess any bumpy structures, but only exhibit a smooth slope for all targets considered here.

Finally, we present energy integrated cross sections $\frac{d\sigma}{d\Omega}$ for kaonic nuclear $1s$ state formation for ^{12}C and ^{28}Si targets with the results obtained in Refs. 10) and 17). We found that our results with the phenomenological optical potential qualitatively agree with those in Ref. 10) and are smaller than those in Ref. 17). The present results with the chiral unitary potential are significantly larger than those with the phenomenological potential because of the smaller momentum transfer in the (K^-, p) reactions due to the smaller binding energies of kaonic nuclear $1s$ states.

Table IV. Energy integrated cross sections for the formation of kaonic $1s$ nuclear states in units of $[\mu\text{b}/\text{sr}]$. The results in Refs. 10) and 17) are also shown for comparison. Proton hole states are $[1p_{3/2}]^{-1}$ and $[1d_{5/2}]^{-1}$ for ^{12}C and ^{28}Si targets, respectively.

Target nucleus	$(d\sigma/d\Omega)_{(K^-, p)} [\mu\text{b}/\text{sr}]$			
	Chiral Unitary	Phenomenology	Ref. 10)	Ref. 17)
^{12}C	425	65	47	100–490
^{28}Si	92.6	2.7	6.0	35–180

§4. Conclusion

We have studied the structure and formation of kaonic atoms and kaonic nuclei in this paper. We used two different kaon-nucleus optical potentials, which are obtained from the chiral unitary model and a phenomenological fit of existing kaonic atom data. We theoretically studied the structure of kaonic atoms and kaonic nuclei using these potentials and determined the differences between the obtained level schemes of the kaonic nuclear states.

We also studied the formation cross sections of deeply bound kaonic atoms and kaonic nuclei which cannot be observed with standard X-ray spectroscopy. All the atomic states are theoretically predicted to be quasi-stable. We investigate the (K^-, p) reaction theoretically and evaluate the cross section of the $^{40}\text{Ca}(K^-, p)$ reaction in detail. For deep atomic state formation, the cross sections are predicted to be approximately $7 [\mu\text{b}/(\text{sr MeV})]$ at $T_K = 20$ and 100 MeV and $2 [\mu\text{b}/(\text{sr MeV})]$ at 400 MeV for kaonic atom $1s$ state formation. For the atomic $2p$ state, the cross section is predicted to be approximately $24 [\mu\text{b}/(\text{sr MeV})]$ at $T_K = 100$ MeV.

We also systematically studied the formation cross sections of kaonic nuclear states in (K^-, p) reactions for various targets. In order to take into account the phase space suppression effects of the decay widths, we introduced a phase space factor to obtain the (K^-, p) spectra. We found in our theoretically studies that in

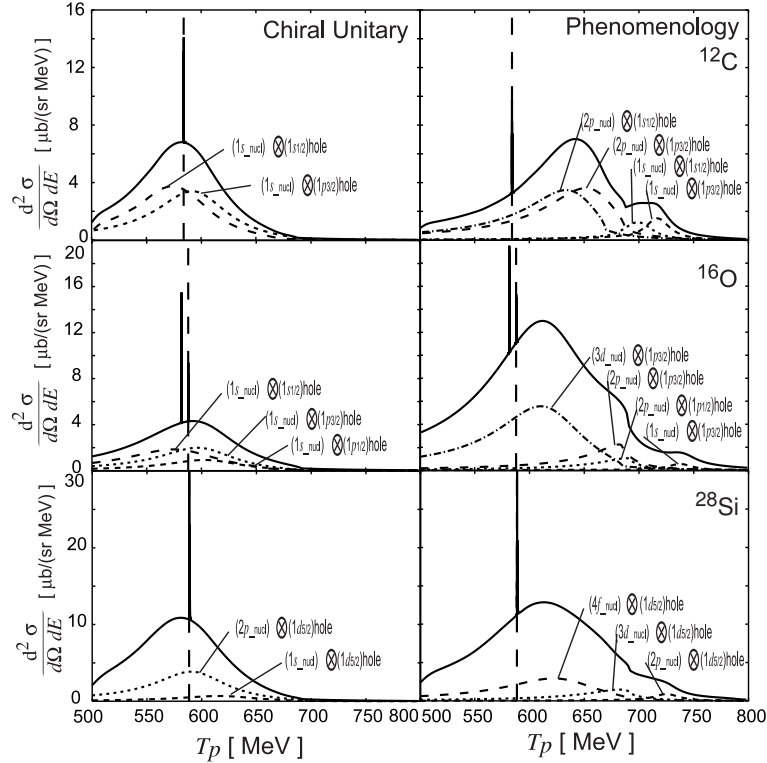


Fig. 11. Same as Fig. 10, except that here the target nuclei are (top) ^{12}C , (middle) ^{16}O , and (bottom) ^{28}Si .

the (K^- , p) reactions, a certain bumpy structure due to kaonic nucleus formation can be seen only for the case of a deep (~ 200 MeV) phenomenological kaon nucleus potential. Due to the phase space suppression, the decay widths of kaonic states become so narrow that we can see certain bumpy structure in the reaction spectrum, which could be seen in experiments. For the case of the chiral unitary potential, the binding energies are too small to reduce the decay widths and to see the bumpy structure in the spectra of the (K^- , p) reactions. However, we should properly include the energy dependence of the chiral unitary potential in future studies of kaonic nuclear states to evaluate more realistic formation spectra.

In order to obtain more conclusive theoretical results, we need to apply Green function methods for states with large widths⁴¹⁾ and to consider the energy dependence of the optical potential properly. Furthermore, we should consider the changes and/or deformations of the nucleus due to the existence of the kaon inside and solve the problem in a self-consistent manner for kaonic nucleus states. However, we believe that the present theoretical effort to evaluate the absolute cross sections for the kaonic bound state formation are relevant for determining a suitable method to observe them and helpful for developing the physics of kaon-nuclear bound systems and kaon behavior in nuclear medium. Further investigations both theoretically and experimentally are needed to understand kaon behavior in nuclear medium more

precisely.

Acknowledgements

We acknowledge E. Oset and A. Ramos for stimulating discussions on kaon bound systems and the chiral unitary model. We would like to thank M. Iwasaki and T. Kishimoto for stimulating discussions on the latest experimental data of kaonic nucleus formation. We also would like to thank T. Yamazaki, Y. Akaishi, and A. Doté for useful discussions on theoretical aspects of kaonic nucleus systems. We are grateful to H. Toki and E. Hiyama for many suggestions and discussions regarding the kaon-nucleus systems. We also thank A. Gal for his careful reading of our preprint and useful comments. This work is partly supported by Grants-in-Aid for scientific research of MonbuKagakusho and Japan Society for the Promotion of Science (No. 16540254).

References

- [1] M. Alberg, E. M. Henley and L. Wilets, *Ann. of Phys.* **96** (1976), 43.
- [2] R. Brockmann, W. Weise and L. Tauscher, *Nucl. Phys.* **A 308** (1978), 365.
- [3] M. Mizoguchi, S. Hirenzaki and H. Toki, *Nucl. Phys.* **A 567** (1994), 893.
- [4] C. J. Batty, *Nucl. Phys.* **A 372** (1982), 418.
- [5] N. Kaiser, P.B. Siegel and W. Weise, *Nucl. Phys.* **A 594** (1995), 325.
- [6] E. Oset and A. Ramos, *Nucl. Phys.* **A 635** (1998), 99.
- [7] T. Waas, N. Kaiser and W. Weise, *Phys. Lett.* **B 365** (1996), 12; **B 379** (1996), 34.
T. Waas and W. Weise, *Nucl. Phys.* **A 625** (1997), 287.
- [8] M. Lutz, *Phys. Lett.* **B 426** (1998), 12.
- [9] A. Ramos and E. Oset, *Nucl. Phys.* **A 671** (2000), 481.
- [10] A. Cieplý et al., *Nucl. Phys.* **A 696** (2001), 173.
- [11] L. Tolós et al., *Nucl. Phys.* **A 690** (2001), 547.
- [12] L. Tolós et al., *Phys. Rev.* **C 65** (2002), 054907.
- [13] S. Hirenzaki, Y. Okumura, H. Toki, E. Oset and A. Ramos, *Phys. Rev.* **C 61** (2000), 055205.
- [14] E. Friedman and A. Gal, *Phys. Lett.* **B 459** (1999), 43.
- [15] E. Friedman and A. Gal, *Nucl. Phys.* **A 658** (1999), 345.
- [16] J. Nieves and E. Oset, *Phys. Lett.* **B 282** (1992), 24.
- [17] T. Kishimoto, *Phys. Rev. Lett.* **83** (1999), 4701.
- [18] T. Kishimoto et al., *Prog. Theor. Phys. Suppl. No.149* (2003), 264.
- [19] M. Iwasaki et al., *nucl-ex/0310018*.
- [20] T. Suzuki et al., *Phys. Lett.* **B 597** (2004), 263.
- [21] Y. Akaishi and T. Yamazaki, *Phys. Rev.* **C 65** (2002), 044005.
- [22] A. Doté, H. Horiuchi, Y. Akaishi and T. Yamazaki, *Phys. Lett.* **B 590** (2004), 51.
- [23] H. Toki and T. Yamazaki, *Phys. Lett.* **B 213** (1988), 129.
H. Toki, S. Hirenzaki, R. S. Hayano and T. Yamazaki, *Nucl. Phys.* **A 501** (1989), 653.
- [24] S. Hirenzaki, H. Toki and T. Yamazaki, *Phys. Rev.* **C 44** (1991), 2472.
H. Toki, S. Hirenzaki and T. Yamazaki, *Nucl. Phys.* **A 530** (1991), 679.
- [25] H. Gilg et al., *Phys. Rev.* **C 62** (2000), 025201.
- [26] K. Itahashi et al., *Phys. Rev.* **C 62** (2000), 025202.
- [27] C. J. Batty, E. Friedman and A. Gal, *Phys. Rep.* **287** (1997), 385.
- [28] E. Oset and L. L. Salcedo, *J. Comput. Phys.* **57** (1985), 361.
- [29] J. Nieves, E. Oset, C. Garcia-Recio, *Nucl. Phys.* **A 554** (1993), 509.
- [30] Review of Particle Physics, Particle Data Group, *Phys. Lett.* **B 592** (2004), 1.
- [31] S. L. Belostotskii et al., *Sov. J. Nucl. Phys.* **41** (1985), 6.
- [32] M. Yosoi et al., *Nucl. Phys.* **A 738** (2004), 451.
- [33] F. Ajzenberg-Selove, *Nucl. Phys.* **A 523** (1991), 1.

- [34] J. Mougey et al., Nucl. Phys. **A 262** (1976), 461.
- [35] U. Amaldi et al., Phys. Rev. Lett. **13** (1964), 341.
- [36] K. Nakamura et al., Phys. Rev. Lett. **33** (1974), 853.
- [37] R. B. Firestone et al., Table of Isotopes, 8th edition (John Wiley & Sons, Inc. ,1996)
- [38] J. Mareš, E. Friedman and A. Gal, Phys. Lett. **B 606** (2005), 295.
- [39] Y. Okumura, Master Thesis, Nara Women's University (2000).
- [40] T. Kishimoto, private communication.
- [41] O. Morimatsu and K. Yazaki, Nucl. Phys. **A 435** (1985), 727; Nucl. Phys. **A 483** (1988), 493.